European Journal of Pharmaceutics and Biopharmaceutics 184 (2023) 139–149

Contents lists available at ScienceDirect

European Journal of Pharmaceutics and Biopharmaceutics

journal homepage: www.elsevier.com/locate/ejpb

Research paper

Co-amorphous formulation of dipyridamole with p-hydroxybenzoic acid: Underlying molecular mechanisms, physical stability, dissolution behavior and pharmacokinetic study

Wei Guo [1], Xueqing Dong [1], Yuanchun Li, Congwei Li, Yawen Tian, Huibing Gao, Tiantian Li, Hanruo Zhu, Jing Wang [*], Caiqin Yang [*]

School of Pharmacy, Key Laboratory of Innovative Drug Development and Evaluation, Hebei Medical University, Shijiazhuang 050017, People's Republic of China

ARTICLE INFO

Keywords:
Dipyridamole
Co-amorphous system
Physicochemical properties
Intermolecular interactions
Glass transition kinetics
Pharmacokinetic study

ABSTRACT

Coamorphization has been proven to be an effective approach to improve bioavailability of poorly soluble active pharmaceutical ingredients (APIs) by virtue of solubilization, and also contributes to overcome limitation of physical stability associated with amorphous drug alone. In current work, a co-amorphous formulation of dipyridamole (DPM), a poor solubility drug, with p-hydroxybenzoic acid (HBA) was prepared and investigated. At a molar ratio of 1:2, DPM and HBA were melted result in the formation of a binary co-amorphous system. The DPM-HBA co-amorphous was structurally characterized by powder X-ray diffraction (PXRD), temperature modulated differential scanning calorimetry (mDSC), high performance liquid chromatography (HPLC) and solution state ^{1}H nuclear magnetic resonance (^{1}H NMR). The molecular mechanisms in the co-amorphous were further analysed via Fourier-transform infrared (FTIR) and Raman spectroscopies, as well as density functional theory (DFT) calculation. All the results consistently revealed the presence of hydrogen bonding interactions between –OH of DPM and −COOH on HBA. Accelerated test and glass transition kinetics showed excellent physical stability of DPM-HBA co-amorphous compared with amorphous DPM along with glass transition temperatures (T_g). The phase-solubility study indicated that complexation occurred between DPM and HBA in solution, which contributed to the solubility and dissolution enhancement of DPM in co-amorphous system. Pharmacokinetic study of co-amorphous DPM-HBA in mouse plasma revealed that the DPM exhibited 1.78-fold and 2.64-fold improvement in $AUC_{0-\infty}$ value compared with crystalline and amorphous DPM, respectively. This current study revealed coamorphization is an effective approach for DPM to improve the solubility and biopharmaceutical performance.

1. Introduction

An increasing number of drug candidates with perfect in vitro pharmacological activity were reported, but the new drugs on the market has not increased in the same proportion [1]. In addition to satisfied biological activity, for drug development, physicochemical properties are also important factors determining its development and listing [2–4]. To optimize physicochemical properties of known active pharmaceutical ingredients (APIs) has been a universal strategy for pharmaceutical research. Among the many properties to be considered, bioavailability and stability are two of the most important parameters during the early stage of drug development [5–7].

Solubility is the basic condition about oral dosage forms to achieve effective treatment concentration, poor solubility directly hinders the absorption and results in low bioavailability of drugs in vivo. Improving the bioavailability by solubility enhancement is an effective and simple way to bring efficacious drugs [8,9]. Based on this, a number of formulation technologies have been developed for the solubilization of drug candidates [5,10–12]. Compared to the long range ordered crystalline forms, amorphous phases with higher free energy and entropy attracted more attention, a large number of water-insoluble crystalline APIs improved the solubility by amorphous transition [13–15]. However, the thermodynamically unstable nature of unary amorphous solids leading to the physical instability during manufacturing and storage.

* Corresponding authors.
E-mail addresses: jingwang@home.ipe.ac.cn (J. Wang), yangcaiqin@hebmu.edu.cn (C. Yang).
[1] The authors contributed equally to this work.

https://doi.org/10.1016/j.ejpb.2023.01.018
Received 6 November 2022; Received in revised form 2 January 2023; Accepted 23 January 2023
Available online 26 January 2023
0939-6411/© 2023 Elsevier B.V. All rights reserved.

Thus, the combination strategy of amorphous drugs with excipients is accepted to enhance both physical stability and aqueous solubility. Among them, amorphous solid dispersion technique is most commonly applied, where an API is molecularly incorporated into polymer carriers [16,17]. In addition to its advantages of solubilization and stability, there are also several disadvantages since the macromolecular polymer introduced to this solid form, including incompatibility, high polymer: drug ratio and hygroscopicity [18,19]. In the recent decade, an alternative strategy, in which the polymeric excipient was replaced by small molecular precursor, to generate new solid forms called co-amorphous. This approach not only can supply solubility advantages and stabilize the amorphous system, but also overcome limitations associated with solid dispersions [20,21].

Dipyridamole (DPM), a phosphodiesterase inhibitor, has been clinically used for prevention and treatment of thromboembolic complications and coronary heart disease [22]. Recent research has reported it also brought benefits for proliferation inhibition, antioxidant, antitumor and anti-inflammatory properties, shows great potential in "new use of old drugs" [23–25]. As a biopharmaceutics classification system (BCS) class II drug, DPM has poor and variable oral absorption with absolute oral bioavailability of 11~44 % [26]. Due to its basic nature (pKa = 6.4), DPM presents pH-dependent solubility and low aqueous solubility (5 μg/mL) at pH 7.0 under body temperature, but dissolves readily in acidic pH and precipitates at basic condition [27]. So far, various formulation techniques, such as salt formation [28], amorphous solid dispersion [29], micronization [30], microenvironmental pH-modifiers [31] and cyclodextrin complexation [32] have already been performed with focus on dissolution, controlled/sustained release and distribution of DPM, whereas promising co-amorphous attempt has not seen, not to mention physicochemical and biopharmaceutical properties. As an analogue of the purine and pyrimidine nucleosides, DPM has abundant H-bond donor and acceptor groups favor the formation of combination system with especially carboxylic acid coformers, supplying structural advantages to form co-amorphous formulation. The p-hydroxybenzoic acid (HBA) is an important target supramolecular synthon of active drugs with functions of optimizing the physicochemical properties in solid state, and widely exists in food, cosmetics and medicine for anti-corrosion, anti-mildew and bactericide [33].

The current work screened a novel DPM-HBA co-amorphous combination which was evaluated systematically in vitro and in vivo. Spectroscopic techniques, thermal analysis and DFT simulation calculation were used to confirm its formation, purity and underlying molecular mechanisms. For the purposes of physical stability evaluation, accelerated tests and glass transition kinetics of the prepared co-amorphous were carried out in comparison to amorphous DPM. Meanwhile, the solubilization by coamorphization was reflected by apparent solubility, as well as the mechanism was researched by phase solubility study. At last, the bioavailability evaluation of the new solid form by the pharmacokinetic study in mouse model.

2. Experimental section

2.1. Materials

Dipyridamole (DPM, Solarbio Science & Technology Co., ltd., Beijing, China), p-hydroxybenzoic acid (HBA, J&K Scientific ltd., Beijing, China), were used as model compounds. The chemical structures of DPM and coformer HBA are shown in Fig. 1. Chlorzoxazone (used as internal HPLC standard) was purchased from Solarbio Science & Technology Co., ltd., Beijing, China. HPLC grade methanol was purchased from Tedia Company Inc. (Ohio, USA). The purity of the DPM obtained was confirmed by DSC and PXRD analyses. All the other solvents were purchased from J&K and without additional purification before use. The water used is deionized water.

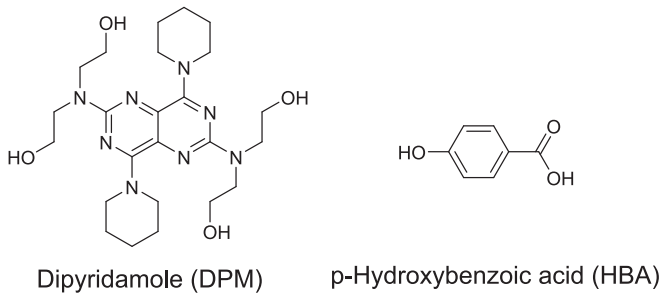


Fig. 1. Chemical structures of dipyridamole (DPM) and p-hydroxybenzoic acid (HBA).

2.2. Preparation of amorphous DPM

The preparation of amorphous DPM was based on a method previously developed in our group [34]. Briefly, 100.0 mg DPM in a quartz boat were heat treated using tubular furnace (Tongda experimental furnace factory, Tianjin, China) from 30 to 190 °C at 5 °C/min. Then the sample naturally cooled down and reheated to 190 °C. The solid was collected after quench cooling over a crushed ice bed and vacuum-stored at room temperature.

2.3. Preparation of DPM-HBA co-amorphous system and physical mixture

The co-amorphous system comprising DPM and HBA were screened using different methods. (1) Melting method: mixtures of crystalline DPM and crystalline HBA with different molar ratios of 1:2, 1:1 and 2:1 (total mass about 100.0 mg) were added into quartz boat and heated using tubular furnace at 150 °C for 5 min. The solid was quench cooled over a crushed ice bed and stored in a vacuum desiccator after drying in a vacuum oven. (2) Solvent evaporation: DPM and HBA formulated with molar ratios of 1:1, 1:2, and 2:1 (total mass about 500.0 mg) were dissolved in 20 mL of various organic solvent (absolute ethanol and acetone). After ultrasonic dissolution at room temperature for 20 min, the solutions were stirred in a 60 °C water bath for 30 min, then evaporated the solvent naturally at room temperature. Yellow sample was obtained and dried in a vacuum. (3) Liquid-assisted ground: mixtures of DPM and HBA at above molar ratios (total mass of 100 mg) were ground in a ball mill (Mixer Mill GT200, Grindertech GmbH, Beijing, China) with a 35 mL zirconia grinding jar and zirconia grinding ball at speed of 1500 rpm. During grinding procedure, 0.2 mL ethanol was dropped to the grinding jar every 5 min to keep the solid in slurry state. After grinding for 30 min, the collected product was dried in a vacuum oven and stored in a vacuum desiccator. All the resultant sample was sieved with 200 mesh screen before used.

The corresponding crystalline physical mixtures of DPM and HBA with the screened molar ratio of 1:2 was prepared in a quartz mortar by mixing with the pestle for 2 min.

2.4. Powder X-ray diffraction (PXRD)

The PXRD experiments were carried out on a SmartLab SE X-ray diffractometer (Rigaku, Tokyo, Japan). The system was equipped with a Cu Kα radiation source (λ = 1.54 Å) and was operated at ambient temperature with 40 kV and 50 mA. All samples were scanned in the reflectance mode from 5 to 40° in 2θ with a scan rate of 4 °/min and a step size of 0.04°.

2.5. Thermal analysis

2.5.1. Differential scanning calorimetry (DSC)

DSC was carried out on a NETZSCH DSC 214 instrument (NETZSCH,

Selb, Germany) attached with a refrigerated cooling accessory (IC40) and a data analyzer (Proteus Analysis 7.0). Before test, the temperature and enthalpy of the instrument was calibrated with an indium standard. Powder samples (5~6 mg) were heated in sealed aluminum pans from 20 to 220 °C at a heating rate of 10 °C/min. Nitrogen was used as the purging gas with flow rate of 40 mL/min. The glass transition kinetics study was carried out under non-isothermal conditions with different heating rates (β) of 5, 10, 15, 20 and 30 °C/min.

2.5.2. Modulated differential scanning calorimetry (mDSC)

mDSC programs using the same instrument of DSC were modulated at 0.5 °C every 60 s in the range of –20 to 170 °C with a heating rate of 2 °C/min. The midpoint temperature on the reversing heat flow profile was seen as the glass-transition temperature (T_g).

2.5.3. Thermogravimetric (TG) analysis

TG analysis of samples was measured using a TG 209 instrument (NETZSCH, Selb, Germany) at a heating rate of 10 °C/min, scanning from 25 to 550 °C under nitrogen purge at a flow rate of 20 mL/min.

2.6. Purity evaluation

2.6.1. High performance liquid chromatography (HPLC).

The analysis was performed on an Agilent Series 1200 (Agilent, Palo Alto City, USA) liquid chromatograph equipped with ultraviolet (UV) detector and connected to Agilent ChemStation software. An Agela reversed-phase C_{18} Column (150 × 4.6 mm, 5 μm) was used and the column temperature was maintained at 25 °C. All the samples were separated using mobile phase consisting of methanol and aqueous with a ratio of 70:30 (v/v). The flow rate was 1 mL/min, and the injection volume was 20 μL. The detection wavelengths for DPM and HBA were set at 284 and 256 nm, respectively.

The stoichiometry relationship between DPM and HBA in co-amorphous mixture was determined using the external standard method via HPLC technique.

2.6.2. Solution state ^1H nuclear magnetic resonance (NMR).

The ^1H NMR characterizations of DPM, HBA, and co-amorphous DPM-HBA were performed on a WIPM NMR-400 spectrometer (Q.One Instruments ltd., Wuhan, China) in 500 μL DMSO-d_6 at room temperature. The spectral width was set as 11013 Hz. The scan number was 16, and the relaxation time D1 was 1 s. Chemical shifts (δ) were calibrated by using TMS as an internal standard and shown in ppm.

2.7. Fourier-transform infrared (FTIR) spectroscopy

The FTIR spectra were recorded with a Prestige-21 FTIR spectrophotometer (Shimadzu Co., Kyoto, Japan). The samples were obtained by grinding 4 mg sample with 160 mg spectral grade KBr in an agate mortar. The scan operated at 2 cm^{-1} resolution and by 16 scans in the region of 400–4000 cm^{-1}.

2.8. Raman spectroscopy

Raman spectra of samples were obtained by the ATR3110 Raman spectrometer (Optosky, Xiamen, China) using a 785 nm excitation laser. The spectra of all samples were recorded over a range of 400–2000 cm^{-1} with a resolution of 2 cm^{-1}.

2.9. Density functional theory (DFT) simulation

The geometry optimizations of DPM and HBA were performed by employing the density functional theory (DFT) method with the Gaussian 09 program [35]. The initial structures of DPM and HBA were created from the Cambridge Structural Database (with CCDC No. 1111518 and 1562101, respectively) and then the geometries of the co-amorphous DPM-HBA at ratio of 1:2 were optimized with the MMFF94 force field followed by geometrical optimization using the density functional theory (DFT) with the B3LYP functional and 6-31G(d,p) basis set. The energy minimization optimization and frequency analysis of the solid state system are carried out to obtain the three-dimensional conformations of these molecules with minimum potential energies.

2.10. Accelerated stability test

The accelerated stability was conducted by exposing the amorphous DPM and co-amorphous DPM-HBA powders in a constant temperature/humidity of 40 °C/75% RH for up to 8 weeks. Samples were collected at predetermined time of 0 h, 24 h, 1 week, 2 weeks, 3 weeks, 4 weeks, 5 weeks, 6 weeks, 7 weeks and 8 weeks to investigate the stability of amorphous materials by PXRD. The crystallization can be monitored by the appearance of the peaks from the amorphous halo in the diffractogram, which was used to evaluate the stability of amorphous samples.

2.11. Solubility determination

2.11.1. Apparent solubility determination

The apparent solubility of DPM-HBA co-amorphous, physical mixture, crystalline and amorphous DPM in 0.1 mol/L pH 6.8 PBS was determined by shake-flask method. An excess of each sample was added to 30 mL 0.1 mol/L pH 6.8 PBS, the suspension was kept at different temperatures of 25 ± 0.5 and 37 ± 0.5 °C and continuously shaken at a constant speed of 150 r/min for 72 h using a SPH-200B air bath shaker (Shiping Tech. Co., ltd., Shanghai, China). A TU-1950 UV−vis spectrometer (Beijing Purkinje General Instrument Co., ltd., Beijing, China) was used to determine the concentration at 400 nm after filtering the suspension via 0.45 μm microfiltration membrane. The calibration curve with regression equation of $A = 0.0137C$ for DPM was constructed in the range of 1–30 μg/mL ($R^2 > 0.9998$). All tests were carried out in triplicate. The pH of the solution after equilibrium was also tested.

2.11.2. Phase solubility diagram

The phase solubility behavior was studied to investigate the solubilization mechanism of HBA to DPM. Excess powder of crystalline DPM were added to 30 mL 0.1 mol/L PBS solution (pH 6.8) of HBA with various concentrations (1.41, 2.91, 4.35, 5.80, 7.25 and 10.84 mmol/L) in glass vials. After shaken at a constant speed of 150 r/min for 72 h at 37 ± 0.5 °C, suspensions were withdrawn and filtrated through a 0.45 μm microfiltration membrane. The DPM concentration in various HBA solutions was determined by the UV method mentioned above after appropriate dilution.

2.12. Powder dissolution test

The powder dissolution studies for co-amorphous DPM-HBA, physical mixture, crystalline and amorphous DPM were performed using paddle method according to the rotating Chinese Pharmacopoeia on a pharmaceutical RCZ-8 M dissolution tester system (Tiandatianfa Technology, Co., ltd., Tianjin, China). The 0.1 mol/L pH 6.8 PBS solution was used as dissolution media at 37 ± 0.5 °C, and the paddle rotation speed was 100 ± 2 rpm. Accurately weighted samples containing the equivalent of DPM (25 mg) were placed in 900 mL dissolution medium. At specified time points (1, 5, 10, 15, 20, 30, 45, 60, 120, 180, 240, 300 and 360 min), 5 mL of dissolution medium was withdrawn followed by replacement with the same volume of fresh ones. The DPM contents in the collected receptor medium were assessed by the mentioned UV method after filtered via 0.45 μm microfiltration. The pH of the solution after equilibrium was also tested.

2.13. In vivo pharmacokinetic study

In order to explore the influence of optimization properties in vitro

on pharmaceutical performance in vivo, the pharmacokinetic behaviors of DPM as crystalline, amorphous and DPM-HBA co-amorphous were evaluated by Sprague Dawley (SD) rats.

Male SD rats (250 ± 10 g weight) supplied by the Hebei Exinvivo Biotechnology Co., ltd (Shijiazhuang, China) were housed at 22 ± 2 °C and 50 ± 5% relative humidity (RH) under artificial 12 h light and dark conditions with access to water and food ad libitum. The Guide for Laboratory Animal Facilities Care were followed while performing animal studies and sanctioned by Animal Ethics Committee of Hebei Medical University. The SD rats were randomly divided into three groups of five animals: pure crystalline DPM, pure amorphous DPM and DPM-HBA co-amorphous. All the groups at a dose of 200 mg equivalent of DPM/kg of rat body mass were administered orally via oral gavage (drops of edible peanut oil was added in the gastric juice to disperse the drug evenly). Before the experiments, rats were fasted for 12 h to minimize the affection in absorption. Blood (0.5 mL) were taken directly from the eye (retrobulbar venous plexus) at predetermined time points of 0.5, 1, 2, 4, 6, 8, 10, 12, 14, 24, 30, 36, 48 and 72 h post-administration and collected into 1.5 mL heparinized centrifuge tubes. The plasma layer was separated by centrifugation at 4000 rpm for 15 min at 4 °C and stored at −20 °C before analysis.

DPM in plasma samples was extracted as following. The plasma sample was mixed with 40 μL chlorzoxazone internal standard and 0.5 mL methanol. The mixture was vortexed for 120 s and centrifuged at 15,000 r/min at 4 °C for 10 min, the supernatant was collected and dried under N_2. The residue was re-dissolved in 0.2 mL mobile phase, and then vortexed for 60 s and centrifuged at 15,000 r/min at 4 °C for 15 min, the final supernatant was used for DPM content analysis by using Ultrahigh-performance Liquid Chromatography (UHPLC and the method validation was shown in Supporting Information).

The pharmacokinetic parameters were derived according to the plasma drug concentration–time analysis by using noncompartmental pharmacokinetic models (DAS 2.0 software). Different pharmacokinetic parameters, contains maximum plasma concentration (C_{max}), the time needed to reach C_{max} (T_{max}), the mean area under the concentration–time curve ($AUC_{0\text{-}24}$, $AUC_{0\text{-}\infty}$), and the elimination half-life ($t_{1/2}$), were compared between treatments.

2.14. Data analysis

SPSS 21.0 software was used for all statistical data analysis. The difference was considered significant at $P < 0.05$. In the determination of solubility and dissolution rate, a completely randomized *t*-test was used to compare the mean of two samples.

3. Results and discussion

3.1. PXRD

Screen of co-amorphous systems based on DPM and HBA was performed using the solvent evaporation, vibrational ball milling and melting methods with the reactants mixed at molar ratios of 2:1, 1:1 and 1:2. PXRD is a rapid technique can be employed to preliminarily identify the formation of co-amorphous. An amorphous system was considered to have formed if the typical halo was observed in the PXRD pattern, whereas the amorphous system was not to have formed if sharp diffraction peaks were observed. As the PXRD patterns of Fig. 2 shown, amorphization was not observed at the DPM:HBA molar ratios of 1:1 and 2:1 by using any of the solvent evaporation, grinding or melting method.

At the 1:2 DPM/HBA molar ratio, the overlapped diffraction peaks of DPM and HBA crystal were found in the PXRD pattern of physical mixture (Fig. 3f). Significantly, DPM resulted into the co-amorphous phase with HBA under this 1:2 molar ratio by both co-heating and solvent evaporation approaches (Fig. 3c and 3d), whereas the grinding treatment remains crystalline character under this composition (Fig. 3e). Thus, the amorphous combination of DPM and HBA was initially screened by PXRD in the unique 1:2 molar ratio by both melting and solvent evaporation methods.

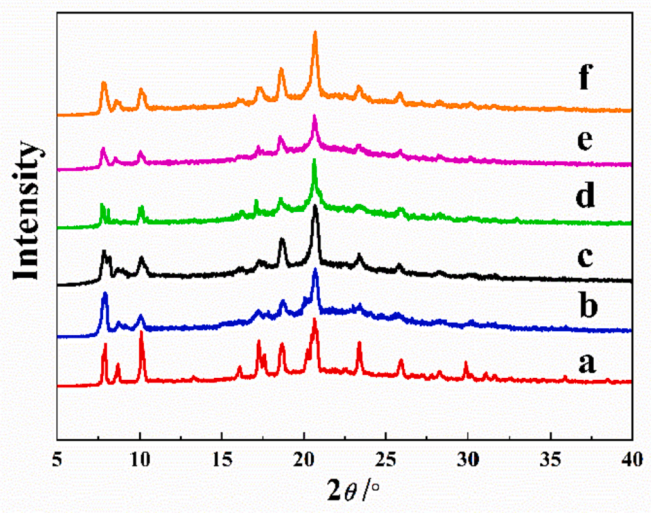


Fig. 2. PXRD patterns of DPM/HBA complex prepared by (a) DPM/HBA 1:1 solvent evaporation, (b) DPM/HBA 2:1 solvent evaporation, (c) DPM/HBA 1:1 grinding, (d) DPM/HBA 2:1 grinding, (e) DPM/HBA 1:1 melting, (f) DPM/HBA 2:1 melting.

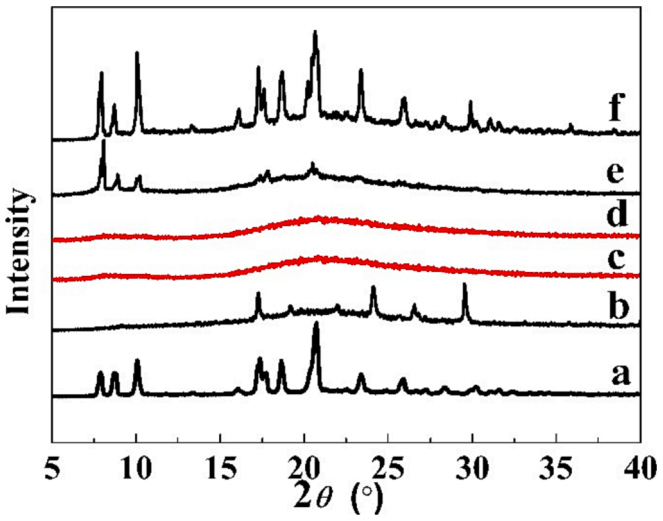


Fig. 3. PXRD patterns of (a) DPM, (b) HBA, and DPM/HBA systems with molar ratio of 1:2 prepared by (c) melting, (d) solvent evaporation, (e) grinding and (f) physical mixture.

3.2. Thermal analysis

mDSC, DSC and TG experiments were utilized to analyze the thermal behavior. As known, PXRD was easily used to identify the amorphous character, but it is insufficient to illustrate whether the composition is a blend of two amorphous raw materials or unique co-amorphous, and even the microcrystallization also show diffraction halo characteristic [36], basically, T_g is a true indicator of the amorphicity of a sample. To further confirm the amorphous nature of the sample, mDSC was performed to identify the T_g of the screened DPM-HBA mixtures prepared by different methods. As shown in Fig. 4, both DPM-HBA complexes showed single T_g at 46.7 °C and 45 °C respectively for the melting and solvent evaporation approach, indicating the formation of homogenous amorphous phase. In contrast, amorphous DPM presented a lower T_g of 38 °C than the combined co-amorphous systems, as we previously

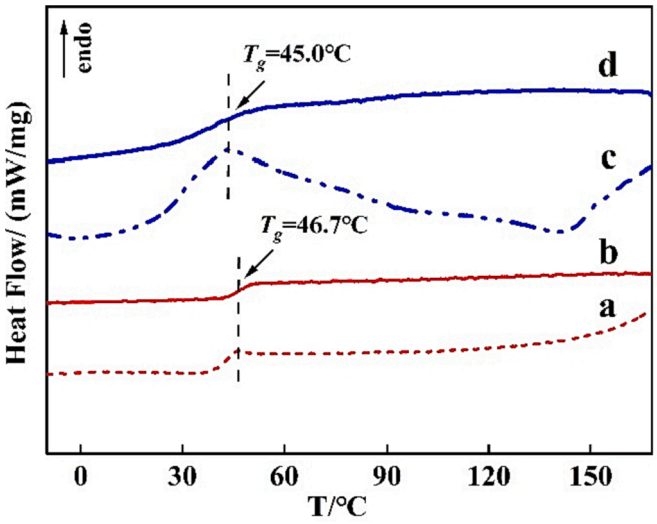


Fig. 4. mDSC curves of DPM-HBA co-amorphous prepared by melting (a) total heat flow, (b) reversing heat flow, and solvent evaporation (c) total heat flow, (d) reversing heat folw.

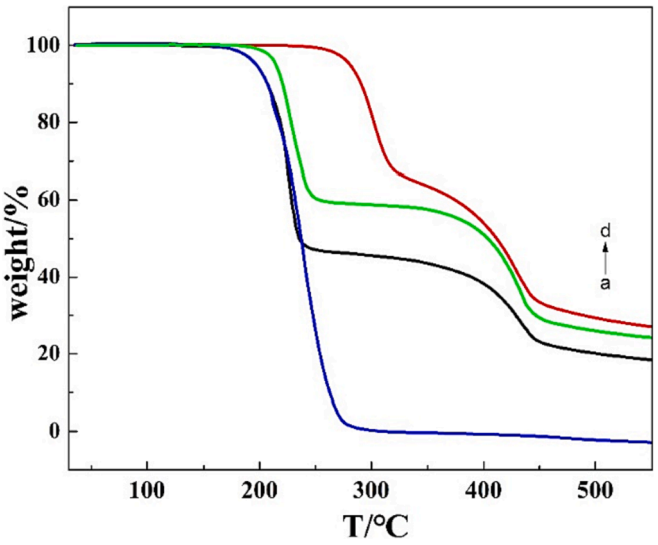


Fig. 6. TG traces of (a) HBA, (b) DPM-HBA co-amorphous, (c) physical mixture and (d) DPM.

reported [34]. Significantly, the two values of T_g are very similar, in view of the long time-consuming of the solvent evaporation method, as well as the possible solvent residue, the DPM-HBA co-amorphous for the following experiments only adopted melting method with DPM:HBA ratio of 1:2.

DSC and TG analysis of crystalline DPM, HBA and their physical mixture, as well as DPM-HBA co-amorphous were employed to explore more thermal properties. As the DSC curves of Fig. 5 shown, sharp fusion endotherms of DPM and HBA crystals presented at 169.9 and 220.3 °C, respectively, consisting with the reported melting points [10]. As previously reported, the broad and low hump was observed on the DSC curve of DPM around 130 °C could be attributed to the solid state transformation of DPM [37]. The DPM-HBA co-amorphous complex showed different thermal behavior from the crystalline reactants, such as the disappearance of the melting point and no new sharp endothermic peak appeared, indicating formation of new solid phase. As Fig. 6 depicted, the distinct mass loss observed in the TG lines can also be considered as evidence for a new phase different from the original components. While the TG curves show no weight loss for all the solids until heating to about 170 °C, indicating the thermal events embodied on the DSC are just states or phases transformation within this temperature range, which further supported the hump located around 130 °C on the DSC curve of DPM was just phase transformation.

Under the ΔpKa rule [38–40], the formed DPM-HBA complex could be either neutral co-amorphous or a salt, with a ΔpKa value of 1.92 (6.40 and 4.48 are respective pKa values of DPM and HBA). Fortunately, the deviation between the experimental T_g and theoretical T_g is regarded as a worth referring parameter to obtain insights on the product formation by symbolizing the molecular interactions in co-amorphous systems [39,41,42]. According to the literature, significant deviation suggesting the stronger interaction between the components and salt formation in the co-amorphous forms. Reversely, no significant deviation indicates weak interaction and means the components were interacted at the molecular level as co-amorphous. Thus then, Fox equation was used to predict theoretical T_g values of DPM-HBA mixture [43]. As a result, the calculated T_g of co-amorphous was 51.2 °C, whereas the T_g of HBA is defined as $0.67T_m$ (T_m: melting point) by the empirical formula [41,44]. By comparison, the experimental T_g (46.7 °C) was in close agreement to the theoretical T_g, supporting that weak interactions between DPM and HBA moieties, that is, the formation of a co-amorphous system but not a salt.

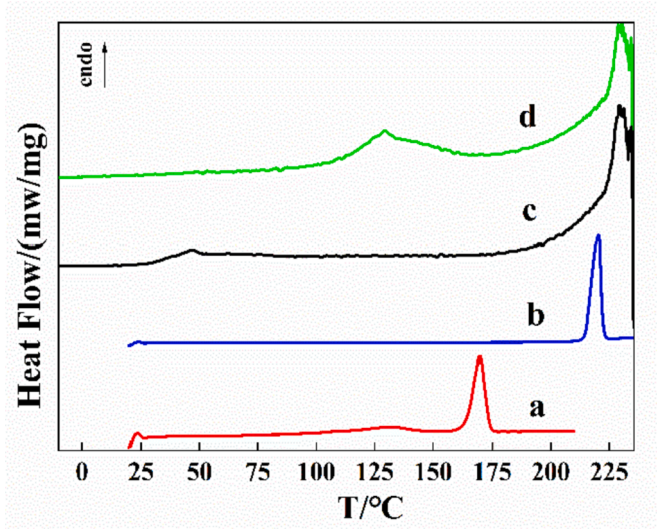


Fig. 5. DSC curves of (a) DPM, (b) HBA, (c) DPM-HBA co-amorphous and (d) physical mixture.

3.3. Purity evaluation

The purity of the synthesized co-amorphous sample was assessed by HPLC and ^{1}H NMR techniques. The product herein was prepared by co-heating, it is very important to detect whether the raw materials decompose in this process.

3.3.1. HPLC

HPLC method is commonly used to judge the purity of samples for those benefits as sensitive and reproducible. The HPLC chromatograms showed the retention time of the HBA was 1.60 min, and the DPM was separated well from HBA with that was 8.05 min (Figure S1). As expected, the absorption peaks of co-amorphous present at 1.60 and 8.04 min, which were basically the same as that of the parent samples. Otherwise, no new peak apparent in the running time.

The stoichiometry of co-amorphous DPM-HBA was also determined by comparing the peak area ratios using the external standard method by HPLC. According the concentration of the two components in co-amorphous, the molar ratio of DPM:HBA equals 1:2.06, which was

consistent with the initial amount of used, further indicating no new substance was generated during preparation.

3.3.2. ^1H NMR

^{1}H NMR also is a sensitive approach to investigate the purity by virtue of the hydrogen number in the complexes. The ^{1}H NMR spectra of parent DPM and HBA compared with the co-amorphous DPM-HBA are shown in Fig. 7 and the chemical shifts and hydrogen numbers are listed in Table S1. The peaks positioned at 2.65 and 3.41 ppm present the solvents of DMSO-d_6 and residual water in it. In the spectrum of DPM, the peaks at 4.72 ppm and 3.61/1.64 ppm were corresponding to hydrogens of O—H and C—H respectively. The chemical shifts at 12.44 and 10.28 ppm were assigned to the signals of active protons in O—H and –COOH, while hydrogens in the benzene ring were observed at 7.81 and 6.84 ppm. In comparison to co-amorphous formation, no extra peak was observed and all the chemical shifts are well assigned and marked in the corresponding spectrum of starting materials. Furthermore, the integral area analysis revealed the hydrogen number ratio of DPM in co-amorphous is equivalent to that of raw materials, but that ratio for benzene ring in DPM-HBA is twice of single HBA, indicating that DPM and HBA are combined in a ratio of 1:2. The hydrogen number ratio of HBA in adduct become smaller than raw HBA, may due to the exchange of active hydrogen between solute and the deuterated water, and do not show a chemical shift peak in the deuterated water solvent.

All the results of HPLC and ^{1}H NMR analysis and quantitative determination demonstrated that prepared co-amorphous DPM-HBA has high purity and the ratio of DPM and HBA combined in 1:2.

3.4. Molecular mechanisms

3.4.1. FTIR spectroscopy

Hydrogen bonding is a common type of weak interactions to promote the combination of molecules, which can lead to the conformational and/or structural variations in functional groups of hydrogen bonding donor and acceptor. FTIR spectroscopy always be performed to gain insight into these possible molecular-level variations.

The medium intensity peaks in the spectrum of DPM with maxima at 3380 and 3311 cm^{-1} can be assigned to the O—H stretching vibrations, and the frequency indicates the existence of homomeric hydrogen bonding [45]; aromatic C═N stretching at 1535 cm^{-1}; C—N stretching at 1360 cm^{-1} and C—H peaks present at 2853 and 2921 cm^{-1} (Fig. 8a). The FTIR spectrum of HBA indicates the characteristic absorption bands at 3386 and 1678 cm^{-1} corresponding to the O—H and C═O vibrations, respectively. Furthermore, the peak located at 927 cm^{-1} suggesting the

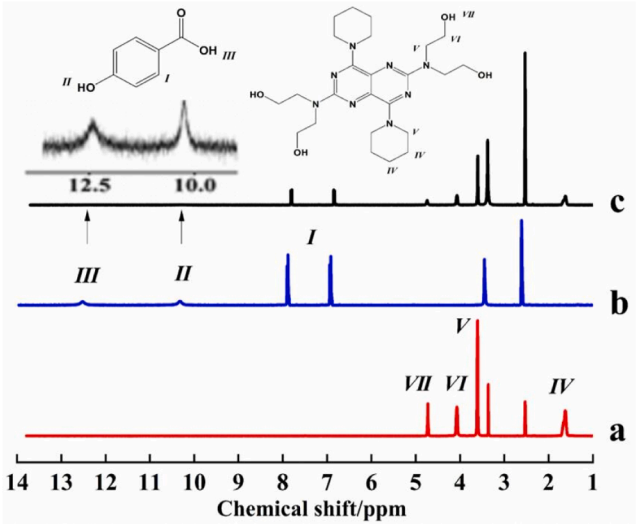


Fig. 7. ^{1}H NMR spectra of (a) DPM, (b) HBA and (c) DPM-HBA co-amorphous.

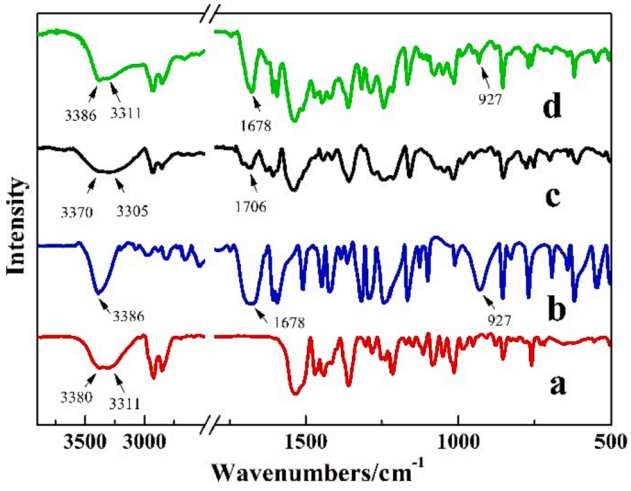


Fig. 8. FTIR spectra of (a) DPM, (b) HBA, (c) DPM-HBA co-amorphous and (d) physical mixture.

HBA molecules affording a homometric dimer (Fig. 8b). These bands mentioned above are the main active groups involved hydrogen bond formation between DPM and HBA. The spectrum of the physical mixture reveals non-shifted peaks of single components, in particular carbonyl peaks (1678 cm^{-1}) and O—H vibrations (3386 and 3311 cm^{-1}, Fig. 8d). In the spectrum of co-amorphous DPM-HBA (Fig. 8c), the stretching of peak due to O—H are merged and broadened suggested the amorphization [46] with slightly shift to 3370–3305 cm^{-1}. The possible reason may due to the intrinsic hydrogen bond in DPM. When HBA was introduced into the lattice of DPM, the homomeric interactions were replaced by the DPM-HBA heteromeric system (co-amorphous). On the other hand, the antisymmetric stretching vibration for the C═O in HBA was blue shifted from 1678 cm^{-1} to 1706 cm^{-1}, and the dimer peak at 927 cm^{-1} disappeared in carboxylic acid dimer. These indicate that the homodimer of HBA molecules were destroyed and then participated in novel hydrogen bonds. Furthermore, there is no characteristic peak for carboxylate, evidencing a neutral amorphous system was formed between DPM and HBA. Based on the analysis above, it can be assumed that the introduction of HBA disrupt the hydrogen bonds between DPM molecules, as well as the HBA homodimers depolymerized. Meanwhile, the C═O and −OH of −COOH in HBA self-assembled with −OH of DPM to form O—H···O═C and O—H···O—H intermolecular hydrogen bonds, which conduced to formation of DPM-HBA co-amorphous.

3.4.2. Raman spectroscopy

Raman spectroscopy is sensitive to the symmetric vibration of nonpolar groups and conformation of organic molecules. It is suitable for the study of drug polymorph, amorphous, isomer and the hydrogen bonding interaction [47]. The Raman spectra for samples in the range from 200 to 2000 cm^{-1} with the emphasis on the –OH and C═O peaks. Crystalline DPM showed its stretching vibration peaks at 857, 863 and 1380 cm^{-1} for –OH and 1572 cm^{-1} for pyrimidine ring (Fig. 9a). Pure HBA showed its stretching vibrations peaks at 837 cm^{-1} for –OH, 1132–1318 cm^{-1} for C—O and 1614 cm^{-1} for C═O (Fig. 9b). Overlapping peaks of crystalline DPM and HBA could be observed in Raman spectrum of physical mixture (Fig. 9d). By way of contrast, the strength, width and position of the peaks of co-amorphous system were changed (Fig. 9c). The spectrum of HBA in the co-amorphous system showed an obvious broaden for the peaks in the region of 1132–1318 cm^{-1}, and the vibration peaks for C—O are merged, suggesting the formation of the disordered structure of the HBA [48]. Meanwhile, the –OH vibrations of both DPM and HBA are merged and shift to 854 cm^{-1}, the peak of pyrimidine ring on DPM is merged with conjugate C═O, C═C groups of HBA and present at 1602 cm^{-1}. These obvious shifts and merger also

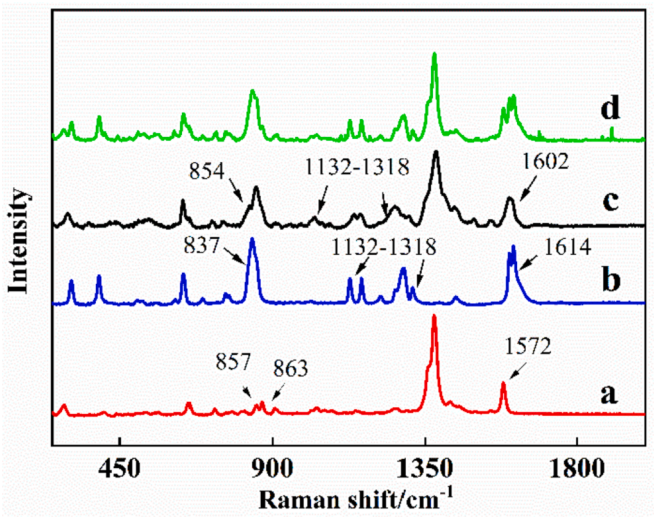


Fig. 9. Raman spectra of (a) DPM, (b) HBA, (c) DPM-HBA co-amorphous and (d) physical mixture.

indicate that the co-amorphous system might be formed via intermolecular hydrogen bonds between –OH of DPM with –COOH of HBA. Similarly, the absence of stretching vibration at 1435–1480 cm^{-1}, which is a characteristic peak for carboxylate, proved the non-salt form of the generated solid system. In summary, the results of the FTIR and Raman spectroscopy study clearly show the existence of intermolecular hydrogen bonds in the co-amorphous system.

3.4.3. DFT calculation

DFT simulation analysis were conducted by Gaussian 09 package to validate the formation of intermolecular hydrogen bonds between DPM and HBA in the co-amorphous system (Fig. 10). The optimized molecular graph with lowest energy of co-amorphous was displayed. It can be seen that the potential hydrogen bond interactions such as C(1)–H(5)···O(6) (H···O distance: 2.96 Å), O(5)–H(6)···O(4) (H···O distance: 1.61 Å), O(2)–H(2)···O(6) (H···O distance: 1.82 Å) and O(5)–H(6)···O(1) (H···O distance: 1.61 Å), supporting the above-mentioned hydrogen bonds deduced from FTIR and Raman spectroscopy. Besides, owing to the weak bonding interactions of C(1)–H(5)···O(6), the corresponding peak shift in FTIR and Raman spectroscopy is not reflected. Thus, the simulation result further confirm and supplement the inference of hydrogen bonding modes in co-amorphous relied on spectral experiments.

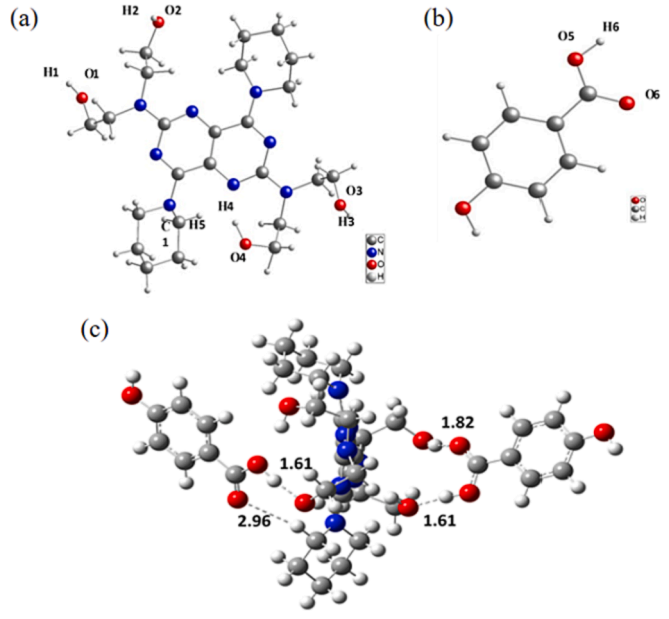


Fig. 10. Crystal structures of (a) DPM, (b) HBA and (c) a simulation diagram of the interaction between DPM and HBA in co-amorphous (the hydrogen bonds were indicated by dotted line and evaluated by bong lengths).

3.5. Accelerated stability

For their higher free energy feature, amorphous solids tend to convert into the stable crystalline counterparts over time under certain temperature and humidity. It is necessary to appraise isothermal crystallization behavior of the amorphous solids. The amorphous DPM nearly complete transferred toward crystalline form after 24 h of storage under 40 °C/75% RH (Figure S2), and further increased crystallinity degree within the tested two weeks. By comparison, the co-amorphous DPM-HBA exhibited an enhanced physical stability at least 1 week under the storage condition, a small crystalline peak corresponding to DPM (7.88° 2θ) could be observed in the PXRD spectrum during storage till second week, and even 8 weeks later just several weak diffraction peaks appeared (Figure S3), but the PXRD pattern maintains the diffraction halo and the recrystallization progress is slow. The results indicated the co-amorphous system displayed a superior physical stability over pure amorphous DPM, which is consistent with the results of glass transition temperature. This may cause by the steric effect and intermolecular interactions produced by introduction of the HBA to DPM moieties.

3.6. Glass transition kinetics of amorphous substances

Non-isothermal method can supply the information about the amorphization ability and stability against devitrification of the amorphous solids [49]. The non-isothermal DSC curves evidenced that T_g of amorphous materials shift higher as the heating rate (β) increases from 5 to 30 °C/min (Figure S4), and the T_g values under different β are listed in Table S2. In the present work, the glass transition kinetics of the two amorphous substances, amorphous DPM and co-amorphous DPM-HBA, were studied by virtue of the dependency of T_g on β using different approaches [50].

The first method is the following an empirical relation that suggested by Lasocka:

$T_g = A + B\ln\beta$.

where A and B are constantsm, $\ln\beta$ is the logarithm of heating rate β. For a certain β, the value of A related to T_g, while the value of B presents the dependence of T_g on β, both the two constants used to reflect the amorphization ability. According to the Lasocka empirical relationship, the resulting straight lines response for T_g *vs* $\ln\beta$ are shown in Figure S5, and the constants A and B deduced from the slopes and intersections of the straight lines were listed in Table 1.

The second approach, derived by Moynihan, suggested that the glass transition temperature varies with the heating rate and the relationship is:

$d(\ln\beta)/d(1/T_g) = -E_t/R$.

where R is the gas constant (8.314 $J{\cdot}K^{-1}{\cdot}mol^{-1}$), and E_t is glass transition activity energy, which is an important parameter that inversely proportional to the stability of the amorphous structures. The

Table 1
Lasocka constants and E_t of amorphous DPM and co-amorphous (n = 3).

Sample	Lasocka constants		E_t (kJ/mol)	
	A/K	B/min	Moynihan	Kissinger
amorphous DPM	302.10 ± 11.36	4.88 ± 0.54	167.00 ± 14.94	161.77 ± 23.70
co-amorphous	308.03 ± 12.13	5.32 ± 0.21	159.55 ± 22.00	154.21 ± 9.29

E_t can be obtained from the slopes of the plots of lnβ as a function of ($1/T_g$) (Figure S6) and the values of the two complexes were listed in Table 1.

The last approach is Kissinger equation, which has been widely used for evaluation of E_t. The equation is given by:

$\partial(\ln T_g^2/\beta)/\partial(1/T_g) = E_t/R$.

Following this method, the values of E_t were calculated from the slopes of the straight lines (Figure S7) $\ln T_g^2/\beta$ *vs* $1/T_g$ and given in Table 1.

It can be seen that the Lasocka constants A and B of the co-amorphous system are greater than those of the amorphous system, indicating the higher formation ability and stability of the co-amorphous system. Besides, the calculated E_t values of amorphous is larger than that of co-amorphous. Judged from this results, the crystallization tendency of co-amorphous is smaller than that of amorphous, that is, stability of co-amorphous is higher [49,50]. Conclusions drawn through the above three approaches showed that co-amorphous formation is more stable than amorphous system, this result is consistent with the accelerated stability tests. One possible reason is the atomic disorder of the co-amorphous system increased after the DPM combined with HBA, leading to more difficult for crystallization by atomic rearrangement. On the other hand, the hydrogen bonding interactions between DPM and HBA reduces the molecular mobility in co-amorphous, and then effectively hinder the crystallization of DPM in supercooled liquid.

3.7. Solubility determination

3.7.1. Apparent solubility

The main advantage of the co-amorphous state is improving solubility of poorly soluble drugs. The apparent solubilities of DPM in crystalline and amorphous forms, the physical mixture and co-amorphous DPM-HBA in 0.1 mol/L pH 6.8 PBS at 25 and 37 °C were illustrated in Fig. 11. As a BCS class II drug, the crystalline DPM exhibited similar solubilities of 3.20 and 3.79 μg/mL respectively at 25 and 37 °C, showed no obvious improvement ($P > 0.05$) under different temperatures. Moreover, the equilibrium concentrations of DPM in physical mixture were 3.69 μg/mL (25 °C) and 4.55 μg/mL (37 °C), showed insignificant difference ($P > 0.05$) for the temperature, as well as with pure crystalline under corresponding conditions. In contrast, the amorphous DPM solubility has dramatically increased with values of 48.58 μg/mL (25 °C) and 50.00 μg/mL (37 °C), which is more than tenfold that of crystalline DPM and the physical mixture, indicating that the solubility of DPM after amorphization is effectively improved. This is because the amorphous characteristic of long-range disordered structure, leading to higher solubility for its high surface energy and free energy. Compared with crystalline form, the solubility of DPM co-amorphous was greatly improved to 51.82 μg/mL (25 °C) and 65.86 μg/mL (37 °C) ($P < 0.01$), slightly higher than that of amorphous at 25 °C ($P > 0.05$) and significantly higher at 37 °C ($P < 0.05$). The enhanced solubility of co-amorphous not only because of the amorphous nature, hydrogen bonding in co-amorphous species also changes the arrangement of DPM molecules, when soluble HBA contact with solvent, it dissolves quickly and improves the hydrophilicity and wettability of DPM simultaneously, so as to promote the dissolution of DPM. At the same time, the determined pH of each system remained at 6.8 when reaching the dissolution equilibrium, which proved that the increase of the solubility of co-amorphous DPM-HBA was not caused by the change of microenvironment because of HBA dissolution, but the dissolution of the two components under the maintenance of intermolecular hydrogen bonds.

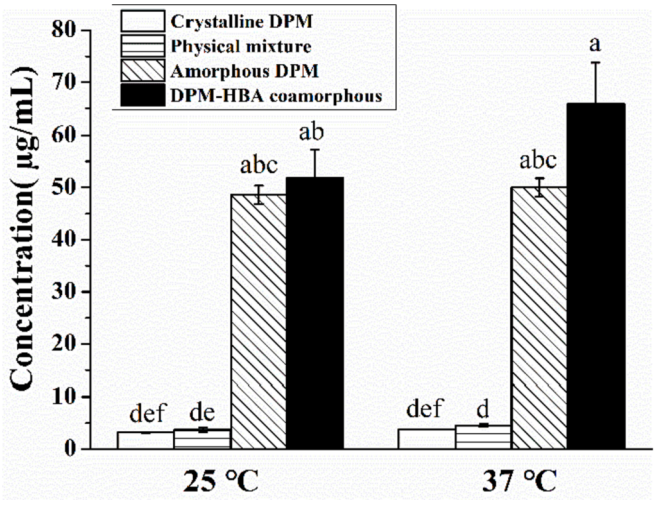


Fig. 11. Solubility profiles of DPM from crystalline drug, the physical mixture of crystalline DPM and HBA, free amorphous and co-amorphous DPM-HBA. Note: The same letter between groups = no significant difference. Note: Different lowercase letters (a-f) indicate significant differences of different samples at the same temperature ($P < 0.05$).

3.7.2. Phase-solubility diagram

Phase-solubility diagram was adopted to elucidate the mechanism of enhancing DPM solubility by HBA [51]. The results showed the phase-solubility diagram of the DPM-HBA system displayed a linear increase in DPM solubility as a function of HBA concentration (Figure S8), featured with an A_L-type with a 1:1 complexation model. Moreover, the calculated complexation constant for the 1:1 complex formed in solution was 28.58.

As discussed above, it is confirmed that the mechanism of DPM-HBA co-amorphous enhanced the solubility of DPM is the complexation between DPM and HBA in solution.

3.8. Dissolution test

In vitro dissolution studies were carried out to investigate the enhanced drug release profiles from the co-amorphous formulation and were compared with free DPM and DPM/HBA physical mixture at 37 ± 0.5 °C in 0.1 mol/L pH 6.8 PBS media (Fig. 12). The dissolution percentage of the co-amorphous system in 6 h is 24.65%, which is about 2.29 times ($P < 0.05$), 4.10 times ($P < 0.05$) and 2.17 times ($P < 0.05$) higher than crystalline DPM, amorphous DPM and physical mixture, respectively. This result is consistent with the solubility tests, confirmed that the co-amorphous system can improve the dissolution of DPM. However, the difference between the dissolution rate of DPM crystal and physical mixture was not obvious ($P > 0.05$), and even the DPM amorphous phase showed a lower dissolution rate compared with the

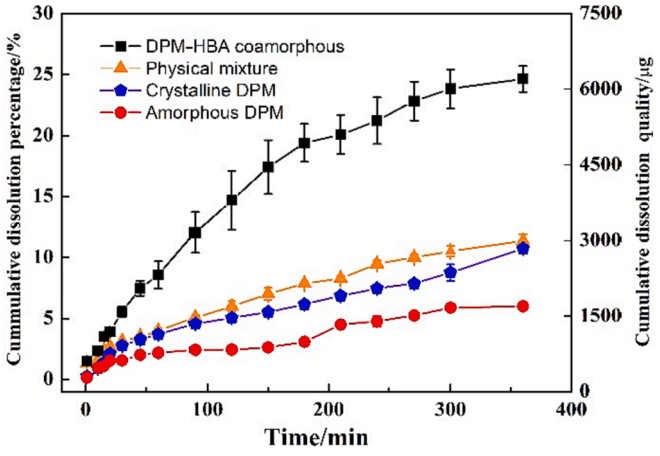


Fig. 12. Powder dissolution profiles of crystalline and amorphous DPM, DPM/HBA physical mixture and DPM-HBA co-amorphous (n = 3).

crystal forms ($P < 0.05$), which may be due to the temperature in solution was close to the T_g value of DPM, the amorphous DPM aggregated in the dissolution medium to form a viscous soft mass, occurs gelation from glass state [52]. The formed gel would adhere to the paddle by the centripetal force of stirring, and inhibit the dissolution. With regard to the co-amorphous sample, due to the increased T_g, it overcomes the transformation to viscous flow state in the dissolution process. By virtue of large unit surface free energy of the amorphous nature, as well as the intermolecular hydrogen bonding optimizes the arrangement of DPM molecules, the co-amorphous dissolution release rapidly, and the dissolution amount increases steadily compared with DPM in crystalline state and physical mixture.

Notably, the results show that the solubility of the amorphous DPM at 37 °C is larger than that of crystalline form, but the dissolution rate is slow. This may be due to the fact that the gelation transition in the early stage of dissolution greatly inhibited the dissolution rate of the drug, resulting in a lower dissolution rate in the determination time, while the dissolution equilibrium process took longer time, and the viscous flow state slowly dissolved but still continued to dissolve. There is no significant difference of amorphous at 37 °C and 25 °C, which may also be explained by gelation.

It can be concluded that the dissolution of DPM is improved after coamorphization. Furthermore, the pH determined of each solution remained at 6.8 when dissolution equilibrium, which further proved that the increase of the in vitro dissolution of co-amorphous due to the complexation rather than change of the pH microenvironment of the system.

3.9. In vivo pharmacokinetic study

The current fully validated UHPLC was succeeded in quantifying the pharmacokinetic parameters of DPM in rat plasma. The main pharmacokinetic parameters of DPM are summarized in Table 2, and the mean plasma concentration–time curves are shown in Fig. 13. It can be found that two-portion absorptions appeared on curves of all the three substances. Part of the reason may be that the liposoluble DPM is partially dissolved in the gastric juice with peanut oil, which is absorbed into the blood and then distributed in the tissue after a long digestion time, then released into the blood again when the blood drug concentration is reduced. On the other hand, DPM itself has a phenomenon of enterohepatic circulation, and the presence of fat stimulates more bile secretion into the intestine, which intensifies the effect of enterohepatic cycle [53,54]. Thus, multiple possible factors work together to trigger the phenomenon of “double peak absorption”.

Compared with crystalline DPM, the pharmacokinetics of amorphous state was not statistically different, and the AUC were even slightly decreased ($P < 0.05$), which were consistent with the results of in vitro dissolution behavior, that is, the dissolution advantage of amorphization did not appear. This may be due to the fact that the body temperature of rat is close to the T_g of amorphous DPM, which makes it gel while metabolize in vivo. However, after the coamorphization with HBA, by virtue of hydrogen bonding interactions, the advantages of dissolution in the body continued for a long time, so as to give better efficacy of the drug.

Table 2
Mean pharmacokinetic parameters of DPM in rats after administration (n = 5).

Parameters	Crystalline DPM	Amorphous DPM	Co-amorphous
C_{max} (μg/L)	1811.002 ± 372.289	1820.512 ± 575.548 ^{ns}	4237.319 ± 1379.785*
T_{max} (h)	12 ± 0.000	10.8 ± 1.095 ^{ns}	10 ± 0.000*
$t_{1/2}$ (h)	13.757 ± 6.022	15.995 ± 3.527 ^{ns}	23.491 ± 13.718*
$AUC_{0\text{-}t}$ (μg/L·h)	24116.747 ± 3516.364	16145.911 ± 4230.476*	41938.349 ± 12928.348*
$AUC_{0\text{-}\infty}$ (μg/L·h)	24792.585 ± 3236.845	16747.027 ± 4318.888*	44176.098 ± 13366.195*

* $P < 0.05$, ns = no significance (*vs* DPM Crystalline).

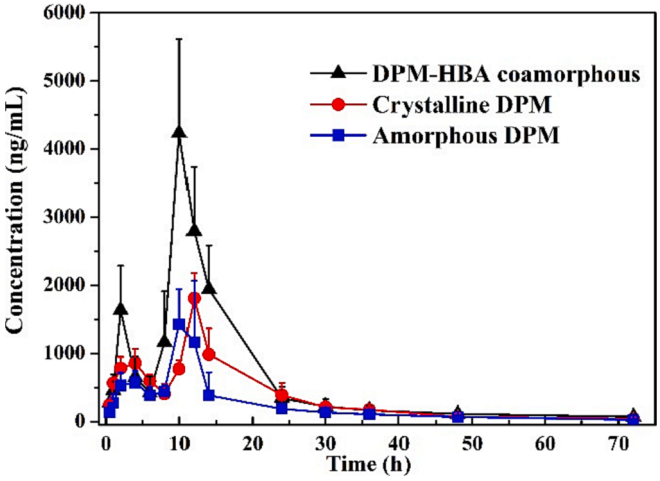


Fig. 13. Mean plasma concentration–time profiles for crystalline DPM, amorphous DPM, and co-amorphous DPM-HBA in rats after administration (n = 5).

As the statistical analysis shown, the DPM in co-amorphous formulation displayed greater pharmacokinetic characteristics compared to free DPM either as crystalline or amorphous. Its T_{max} advanced by 2.0 h and 0.8 h than that of the respectively crystalline ($P < 0.05$) and amorphous DPM, meanwhile, the C_{max} was about 2.3-fold ($P < 0.05$) compared to the single DPM. The mean $AUC_{0\text{-}\infty}$, showed 1.74- and 2.60-fold ($P < 0.05$) improvement in the exposure of co-amorphous DPM over its crystalline and amorphous counterpart. It is mainly emphasized that, not only the C_{max} increased, the $t_{1/2}$ of DPM from the co-amorphous is prolonged by nearly 10 h ($P < 0.05$), which is beneficial to increasing the retention time in vivo to obtain enduring therapeutic effects. All the results indicate that DPM-HBA co-amorphous has faster efficacy, longer action time and higher bioavailability than the single crystalline or amorphous DPM.

4. Conclusion

In conclusion, a DPM-HBA co-amorphous complex was successfully prepared through melting method. Characterization by PXRD and thermal analysis techniques revealed the neutral single phase with a DPM:HBA molar ratio of 1:2, which were further confirmed by purity evaluation via HPLC and ^{1}H NMR experiments. The accelerated stability tests and glass transition kinetics studies revealed the binary co-amorphous formation has higher stability than the homogeneous amorphous system. The underlying molecular mechanisms in the co-amorphous solid were involved in hydrogen bonding between –OH of DPM with −COOH on HBA, which were systematically investigated and identified using spectroscopy and simulation methods. The DPM in co-amorphous formulation significantly increased in solubility and in vitro dissolution than that of in crystal and amorphous, the mechanism of solution enhancement was complexation with HBA. These benefits were successfully translated into in vivo studies leading to the enhancement in the blood plasma concentration from the DPM-HBA co-amorphous as well as prolonged the $t_{1/2}$, which means enhanced oral bioavailability. This study supplied an exploratory strategy to overcome the barriers of the BCS II drug in the oral absorption by coamorphization. From the findings, the combination of polyfunctional drug with a desirable co-former based on the structural characteristics of the drug candidate and physicochemical properties of the obtained co-amorphous samples is a reasonable and promising strategy.

Declaration of Competing Interest

The authors declare that they have no known competing financial

interests or personal relationships that could have appeared to influence the work reported in this paper.

Data availability

Data will be made available on request.

Acknowledgments

This work was supported by the Biological Medicine Joint Fund of Natural Science Foundation of Hebei Province (NO. H2020206128 and H2021206101). The DFT simulation was supported by Professor Dai Y.J. in Tianjin University of Science and Technology, Tianjin, China. Thanks are also due to Hebei Medical University Core Facilities and Centers for PXRD and NMR measurements.

Appendix A. Supplementary data

Supplementary data to this article can be found online at https://doi.org/10.1016/j.ejpb.2023.01.018.

References

[1] P.K. Parmar, J. Wadhawan, A.K. Bansal, Pharmaceutical nanocrystals: a promising approach for improved topical drug delivery, Drug Discov. Today 27 (2021) 1236–1250.
[2] M.C. Wenlock, P. Barton, In silico physicochemical parameter predictions, Mol. Pharm. 10 (2013) 1224–1235.
[3] P. Zarmpi, T. Flanagan, E. Meehan, J. Mann, N. Fotaki, Biopharmaceutical understanding of excipient variability on drug apparent solubility based on drug physicochemical properties: case study—hypromellose (HPMC), AAPS J. 22 (2020) 1–15.
[4] W. Xu, L. Chao, Y. Zhang, P. Quan, L. Fang, An investigation on the effect of drug physicochemical properties on the enhancement strength of enhancer: the role of drug-skin-enhancer interactions, Int. J. Pharm. 607 (2021), 120945.
[5] H.D. Williams, N.L. Trevaskis, S.A. Charman, R.M. Shanker, W.N. Charman, C. W. Pouton, C.J. Porter, Strategies to address low drug solubility in discovery and development, Pharmacol. Rev. 65 (2013) 315–499.
[6] S.R. Byrn, G. Zografi, X. Chen, Accelerating proof of concept for small molecule drugs using solid-state chemistry, J. Pharm. Sci. 99 (2010) 3665–3675.
[7] S.T. Mannully, C. Shanthi, K.K. Pulicherla, Lipid modification of staphylokinase and its implications on stability and activity, Int. J. Boil. Macromol. 121 (2019) 1037–1045.
[8] L. Di, E.H. Kerns, G.T. Carter, Drug-like property concepts in pharmaceutical design, Curr. Pharm. Des. 15 (2009) 2184–2194.
[9] G.L. Amidon, H. Lennernäs, V.P. Shah, J.R. Crison, A theoretical basis for a biopharmaceutic drug classification: the correlation of in vitro drug product dissolution and in vivo bioavailability, Pharm. Res. 12 (1995) 413–420.
[10] M. Maghsoodi, A. Nokhodchi, H.I. Babi, Rational selection of formulation components to improve dissolution of dipyridamole, J. Drug Deliv. Sci. Technol. 55 (2020), 101467.
[11] M.W. Stocker, A.M. Healy, S. Ferguson, Spray encapsulation as a formulation strategy for drug-based room temperature ionic liquids: exploiting drug-polymer immiscibility to enable processing for solid dosage forms, Mol. Pharm. 17 (2020) 3412–3424.
[12] Z. Zhang, Q. Zhang, Q. Zhang, C. Chen, M. He, Q. Chen, G. Song, X. Xuan, X. Huang, From a binary salt to salt co-crystals of antibacterial agent lomefloxacin with improved solubility and bioavailability, Acta Crystallogr. B 71 (2015) 437–446.
[13] J.M. Skieneh, I. Sathisaran, S.V. Dalvi, S. Rohani, Co-amorphous form of curcumin–folic acid dihydrate with increased dissolution rate, Cryst. Growth Des. 17 (2017) 6273–6280.
[14] P. Khadka, S. Sinha, I.G. Tucker, J. Dummer, P.C. Hill, R. Katare, S.C. Das, Pharmacokinetics of rifampicin after repeated intra-tracheal administration of amorphous and crystalline powder formulations to Sprague Dawley rats, Eur. J. Pharm. Biopharm. 162 (2021) 1–11.
[15] B. Emer, Q. Sian, C. Sheena, H.A. Marie, Design and characterisation of an amorphous formulation of nifedipine for the treatment of autonomic dysreflexia, J. Phar. Pharmacol. 73 (2021) 928–936.
[16] S.B. Sapkal, S.A. Shinde, R.A. Darakhe, V.N. Shikhande, Solid dispersion of valsartan for solubility improvement using betacyclodextrin, MOJ Bioequiv. Availab. 5 (2018) 313–319.
[17] D. Medarević, S. Cvijić, V. Dobričić, M. Mitrić, J. Djuriš, S. Ibrić, Assessing the potential of solid dispersions to improve dissolution rate and bioavailability of valsartan: in vitro-in silico approach, Eur. J. Pharm. Sci. 124 (2018) 188–198.
[18] K. Ueda, N. Yamamoto, K. Higashi, K. Moribe, Molecular mobility suppression of ibuprofen-rich amorphous nanodroplets by HPMC revealed by NMR relaxometry and its significance with respect to crystallization inhibition, Mol. Pharmaceutics 16 (2019) 4968–4977.
[19] P. Hoppu, S. Hietala, S. Schantz, A.M. Juppo, Rheology and molecular mobility of amorphous blends of citric acid and paracetamol, Eur. J. Pharm. Biopharm. 71 (2009) 55–63.
[20] S.J. Dengale, H. Grohganz, T. Rades, K. Löbmann, Recent advances in co-amorphous drug formulations, Adv. Drug Deliv. Rev. 100 (2016) 116–125.
[21] Z. Wang, X. Chen, D. Li, E. Bai, H. Zhang, Y. Duan, Y., Platensimycin-berberine chloride co-amorphous drug system: Sustained release and prolonged half-life, Eur. J. Pharm. Biopharm. 179 (2022) 126–136.
[22] H.H. Kim, J.K. Liao, Translational therapeutics of dipyridamole, Arterioscler. Thromb. Vasc. Biol. 28 (2008) s39–s42.
[23] A.E. El-Sisi, S.S. Sokar, H.A. Ibrahim, S.E. Abu-Risha, Enhanced anticancer activity of combined treatment of imatinib and dipyridamole in solid ehrlich carcinoma-bearing mice, Naunyn Schmiedebergs Arch. Pharmacol. 383 (2020) 1113–1129.
[24] M.P. Thomé, L.C. Pereira, G.R. Onzi, F. Rohden, M. Ilha, F.T. Guma, M.R. Wink, G. Lenz, Dipyridamole impairs autophagic flux and exerts antiproliferative activity on prostate cancer cells, Exp. Cell Res. 382 (2019), 111456.
[25] S. Guo, M. Stins, M. Ning, E.H. Lo, Amelioration of inflammation and cytotoxicity by dipyridamole in brain endothelial cells, Cerebrovasc. Dis. 30 (2010) 290–296.
[26] B. Terhaag, F. Donath, G. Le Petit, K. Feller, The absolute and relative bioavailability of dipyridamole from different preparations and the in vitro-in vivo comparison, Int. J. Clin. Pharmacol. Ther. Toxicol. 24 (1986) 298–302.
[27] T.L. Russell, R.R. Berardi, J.L. Barnett, T.L. O'Sullivan, J.G. Wagner, J.B. Dressman, pH-related changes in the absorption of dipyridamole in the elderly, Pharm. Res. 11 (1994) 136–143.
[28] S.B. Vepuri, H.C. Devarajegowda, M.E. Soliman, Synthesis, characterization and molecular modelling of a novel dipyridamole supramolecule – X-ray structure, quantum mechanics and molecular dynamics study to comprehend the hydrogen bond structure-activity relationship, J. Mol. Struct. 1105 (2016) 194–204.
[29] S. Baghel, H. Cathcart, N.J. O'Reilly, An investigation into the solid-state properties and dissolution profile of spray dried ternary amorphous solid dispersions: a rational step towards the design and development of multi-component amorphous system, Mol. Pharm. 15 (2018) 3796–3812.
[30] G.P. Sanganwar, R.B. Gupta, Nano-mixing of dipyridamole drug and excipient nanoparticles by sonication in liquid CO_2, Powder Technol. 196 (2009) 36–49.
[31] Z. Xi, N. Sharma, A. Paprikar, S. Lin, Development and evaluation of dipyridamole sustained release tablets containing micro-environmental pH modifiers, J. Drug Deliv. Sci. Technol. 54 (2019), 101231.
[32] G. Ricevuti, A. Mazzone, D. Pasotti, E. Uccelli, F. Pasquali, G. Gazzani, G. B. Fregnan, Pharmacokinetics of dipyridamole-beta-cyclodextrin complex in healthy volunteers after single and multiple doses, Eur. J. Drug Metab. Pharmacokinet. 16 (1991) 197–201.
[33] H.B. Kostenbauder, T. Higuchi, Formation of molecular complexes by some water-soluble amides interaction of several amides with p-hydroxybenzoic acid, salicylic acid, chloramphenicol, and phenol, J. Phar. Sci. 45 (2010) 518–522.
[34] J. Sun, C. Li, Y. Tian, C. Yang, Evaluation of kinetic stability of dipyridamole amorphous drug system, J. Shihezi U. (Natural Science) 40 (2022) 21–26.
[35] M.J. Frisch, G.W. Trucks, H.B. Schlegel, G.E. Scuseria, M.A. Robb, J.R. Cheeseman, G. Scalmani, V. Barone, G.A. Petersson, H. Nakatsuji, X. Li, M. Caricato, A. Marenich, J. Bloino, B.G. Janesko, R. Gomperts, B. Mennucci, H.P. Hratchian, J.V. Ortiz, A.F. Izmaylov, J.L. Sonnenberg, D. Williams-Young, F. Ding, F. Lipparini, F. Egidi, J. Goings, B. Peng, A. Petrone, T. Henderson, D. Ranasinghe, V.G. Zakrzewski, J. Gao, N. Rega, G. Zheng, W. LiangM. Hada, M. Ehara, K. Toyota, R. Fukuda, J. Hasegawa, M. Ishida, T. Nakajima, Y. Honda, O. Kitao, H. Nakai, T. Vreven, K. Throssell, J.J.A. Montgomery, J.E. Peralta, F. Ogliaro, M. Bearpark, J.J. Heyd, E. Brothers, K.N. Kudin, V.N. Staroverov, T. Keith, R. Kobayashi, J. Normand, K. Raghavachari, A. Rendell, J.C. Burant, S.S. Iyengar, J. Tomasi, M. Cossi, J.M.illam, M. Klene, C. Adamo, R. Cammi, J.W. Ochterski, R.L. Martin, K. Morokuma, O. Farkas, J.B. Foresman, D.J. Fox, Gaussian 09, Revision A. 02 (2016) Gaussian, Inc.: Wallingford CT.
[36] S. Dedroog, T. Pas, B. Vergauwen, C. Huygens, G. Van den Mooter, Solid-state analysis of amorphous solid dispersions: why DSC and XRPD may not be regarded as stand-alone techniques, J. Pharm. Biomed. Anal. 178 (2019), 112937.
[37] V. Berbenni, A. Marini, G. Bruni, A. Maggioni, P. Cogliati, Thermoanalytical and spectroscopic characterization of solid state dipyridamole, J. Therm. Anal. Calorim. 68 (2002) 413–422.
[38] S. Kumar, A. Nanda, Pharmaceutical cocrystals: an overview, Indian J. Pharm. Sci. 79 (2017) 858–871.
[39] X. Shi, B. Fan, C. Gu, X. Zhou, C. Wang, Z. Ding, Ibrutinib and carboxylic acid co-amorphous system with increased solubility and dissolution: a potential interaction mechanism, J. Drug Deliv. Sci. Tec. 59 (2020), 101875.
[40] A.J. Cruz-Cabeza, Acid–base crystalline complexes and the p*K*a rule, CrystEngComm. 14 (2012) 6362–6365.
[41] J. Liu, T. Rades, H. Grohganz, Determination of the optimal molar ratio in amino acid-based co-amorphous systems, Mol. Pharm. 17 (2020) 1335–1342.
[42] H. Ueda, W. Wu, K. Löbmann, H. Grohganz, A. Müllertz, T. Rades, Application of a salt coformer in a co-Amorphous drug system dramatically enhances the glass transition temperature: a case study of the ternary system carbamazepine, citric acid, and L-arginine, Mol. Pharm. 15 (2018) 2036–2044.
[43] T.G. Fox, Influence of diluent and of copolymer composition on the glass temperature of a polymer system, Bull. Am. Phys. Soc. 1 (1956) 123.
[44] S. Sakka, J.D. Mackenzie, Relation between apparent glass transition temperature and liquids temperature for inorganic glasses, J. Non Cryst. Solids 6 (1971) 145–162.
[45] D.E. Braun, R.M. Bhardwaj, A.J. Florence, D.A. Tocher, S.L. Price, Complex polymorphic system of gallic acid−five monohydrates, three anhydrates, and over 20 solvates, Cryst. Growth Des. 13 (2012) 19–23.

[46] A. Heinz, C.J. Strachan, K.C. Gordon, T. Rades, Analysis of solid-state transformations of pharmaceutical compounds using vibrational spectroscopy, J. Pharm. Pharmacol. 61 (2009) 971–988.
[47] L.S. Taylor, F.W. Langkilde, Evaluation of solid-state forms present in tablets by Raman spectroscopy, J. Pharm. Sci. 89 (2000) 1342–1353.
[48] G.P. Andrews, O. Abu-Diak, F. Kusmanto, P. Hornsby, Z. Hui, D.S. Jones, Physicochemical characterization and drug-release properties of celecoxib hot-melt extruded glass solutions, J. Pharm. Pharmacol. 62 (2010) 1580–1590.
[49] O.A. Lafi, Glass transition kinetics and crystallization mechanism in $Se_{90}Cd_8Bi_2$ and $Se_{90}Cd_6Bi_4$ chalcogenide glasses, J. Alloys. Compd. 519 (2012) 123–128.
[50] M.M.A. Imran, Crystallization kinetics, glass transition kinetics, and thermal stability of Se70-xGa30Inx (x=5, 10, 15, and 20) semiconducting glasses, Physica B Condens. Matter 406 (2011) 482–487.
[51] S.J. Nehm, B. Rodríguez-Spong, N. Rodríguez-Hornedo, Phase solubility diagrams of cocrystals are explained by solubility product and solution complexation, Cryst. Growth Des. 6 (2006) 592–600.
[52] J. Ren, W. Heng, S. Zhou, Y. Gao, J. Zhang, Gelation of small molecule amorphous drugs, Acta Pharm. Sin. 56 (2021) 855–864.
[53] R.A. Abbiati, D. Manca, Enterohepatic circulation effect in physiologically based pharmacokinetic models: the sorafenib case, Ind. Eng. Chem. Res. 56 (2017) 3156–3166.
[54] B. Terhaag, F. Donath, G.L. Petit, K. Feller, The absolute and relative bioavailability of dipyridamole from different preparations and the in vitro-in vivo comparison, Int. J. Clin. Pharmacol. Ther. 24 (1986) 298–302.